arXiv:nucl-th/0311106v1 28 Nov 2003

Angular Momentum Projection and Quadrupole Correlations Effects in Atomic Nuclei

J. L. Egido and L. M. Robledo

Departamento de Física Teórica C–XI, Universidad Autónoma de Madrid,
E–28049 Madrid, Spain

1 Introduction

The mean field approach when combined with effective interactions like Skyrme or Gogny is central to the understanding of nuclear structure as it provides the right magic numbers and a rather good description of nuclear properties like masses, radii, etc, see [1] and references therein. In this approach nucleons are assumed to move in orbits created by a common potential and therefore the nuclear wave function for the ground state can be represented as a Slater determinant built upon the orbitals occupied by the nucleons. The common potential is determined from the effective interaction by solving the Hartree- Fock (HF) equation. On the other hand, most of the nuclei show, at least in their ground state, the phenomenon of nuclear superconductivity due to a part of the interaction known as pairing interaction. When this is the case we have to introduce the concept of quasi-particles (given by the canonical Bogoliubov transformation) and the mean field wave function now becomes a product wave function of annihilation quasi-particle operators. The quasi-particle amplitudes are determined by solving the Hartree- Fock- Bogoliubov (HFB) equation.

The nuclear mean field has a strong tendency to show the phenomenon called "spontaneous symmetry breaking" [2, 3, 4] that appears when the HF or HFB wave functions do not respect the underlying symmetries of the Hamiltonian. In fact this is the case, for example, for the HFB wave functions as they do not have a definite number of particles, i.e. they spontaneously break the "number of particles" symmetry. As the atomic nucleus is a finite system the spontaneous symmetry breaking mechanism is a mere artifact of the mean field approximation to generate correlations (although it allows an intuitive understanding of some nuclear structure effects like rotational bands) contrary to what happens in quantum field theory where it represents a real effect due to the infinite number of degrees of freedom. Usually in nuclear physics the spontaneous symmetry breaking has to do with spatial symmetries like the rotational or parity symmetries. In the former case it leads to the concept of "deformed mean field" where the common potential felt by nucleons is not rotational invariant (i.e. it is deformed in opposition to a spherical -rotational invariant- potential) and, as a consequence, the ground state wave function is not an eigenstate of the angular momentum operators J^2 and J_z (i.e. the Casimir operators of the rotation group). However, the real wave function of the nucleus is an eigenstate of angular momentum and therefore it is necessary to go beyond the mean field approximation in order to have the right quantum numbers. The procedure to restore the symmetry is known as the Angular Momentum Projection (AMP) method [5] and relies in the fact that when the "deformed mean field" wave function (in the following the "intrinsic" wave function) is rotated the corresponding intrinsic mean field energy remains the same. Therefore, a suitable linear combination of such rotated "intrinsic states" will recover the angular momentum quantum numbers of the wave function and at the same time will reduce the energy (what is worthy from a variational point of view). Usually it is said in the literature that the "deformed mean field" wave functions belong to the "intrinsic" frame of reference whereas the projected wave functions belong to the "laboratory" frame of reference. In order to go from the intrinsic frame to the laboratory one the fluctuations in orientation have to be added to the intrinsic wave function in exactly the way as it is done in the Angular Momentum Projection framework.

Angular Momentum Projection has been a goal of nuclear physicist for many years and only recently with the new computer facilities has become a reality for involved forces. Apart from the traditional motivations a considerable effort has been made, in the last few years, in order to implement Angular Momentum Projection with realistic effective interactions. The main reason, apart from the genuine desire of always having the best theoretical description, is the wealth of new experimental data in exotic regions of the Nuclide Chart far away from the stability line and coming from the amazing and very sophisticated experimental setups that have been assembled in the last few years. In many cases, the experimental results can not be reproduced or even understood adequately with a mean field description and therefore, in addition to considerations concerning the suitability of such interactions away from the stability line, effects beyond mean field have to be explored. As a result of the AMP calculations it turned out that away of the stability line the potential energy surfaces are very soft and that shape coexistence is a phenomenon rather common in these exotic regions. In these cases one is forced to perform, besides the AMP, configuration mixing calculations. The most effective way to consider shape mixing is the Generator Coordinate Method (GCM) in which the relevant coordinates (in general the multipole moments) are used to generate the corresponding wave functions. The mixing coefficients are obtained by solving the Hill-Wheeler equation [6]. The combined AMPGCM with effective forces is a very powerful method which has allowed, as we will see, to understand and to predict many new features.

Obviously there are many more methods apart from the one to be discussed here that are successful in the description the nuclear structure phenomena at low energies. We have the traditional shell model (see [7] for a recent review and [8] for the state of the art implementations of this method) where first a reduced set of orbitals is chosen as to be the one playing the most important role in the physics to be described and then the full diagonalization of the Hamiltonian in the space of multi particle-hole excitations coupled to the right quantum numbers is performed. Very good results are obtained with this method when the effective interaction used is fine tuned to the set of nuclei to be described and also when the physics to be described lies within the configuration space chosen. However, there are several drawbacks for this method: a) The dimension of the Hamiltonian matrix to be diagonalized dramatically increases with the size of the configuration space restricting its applicability to mass numbers smaller than 70 and also to states that do not involve different major shells at the same time. b) Its success depends upon a careful fitting of the interaction and therefore it is not suited for exploratory calculations in new regions of the Nuclide Chart. c) Finally, it is difficult to recast the results in terms of traditional concepts based on a mean field picture of the nucleus.

Another interesting approach is variational approach of the Tübingen group [9, 10] where the lab frame wave functions of the nucleus are constructed by projecting, onto all the preserved quantum numbers, an unrestricted intrinsic mean field wave function. The method is sometimes complemented by allowing also multi particle-hole excitations which are also variationally determined and then the set of wave functions obtained is used to diagonalize the Hamiltonian. This method fully shares one of the drawbacks of the shell model approach, namely the one denoted by b) in the previous paragraph and it also partially suffers from the drawback a) of the shell model, namely that not so big configuration spaces can be used in the calculations. Up to now it has been possible to study nuclei in the Kr (Z=36) region with this method.

An approach that can be extended to heavy nuclei is the Projected Shell Model (PSM) of Hara and Sun [11]. In this method the Hamiltonian is taken as the one of the Pairing+Quadrupole model with single particle energies fitted to experimental data. The HFB ground state and many multiquasiparticle excitations are projected onto good angular momentum and the Hamiltonian is diagonalized in the resulting basis. One of the advantages of the method over the two previous ones is that bigger configuration spaces can be used (up to three harmonic oscillator major shells) but it shares the deficiency related to the fitting procedure of the interaction in order to get a reasonable description of experimental data.

Finally, we have the Monte Carlo Shell Model (MCSM) approach of Otsuka and collaborators [12]. In this method intrinsic wave functions are generated stochastically and then projected onto the right quantum numbers. The resulting configuration is kept if its projected energy is lower than a given threshold generating in this way a basis of projected wave functions. The Hamiltonian is diagonalized in this basis at the end. As in the other approaches, rather limited configuration spaces can be used (although it is possible to carry out calculations for nuclei as heavy as Barium) and the matrix elements of the interaction have to be carefully fitted to the region of interest.

The four approaches just described share the common problem of the effective charges that have to be introduced in the calculation of transition probabilities as a consequence of the limited configuration spaces.

The main advantage of using beyond mean field approaches with effective forces over the other approaches mentioned before relies in the universal character of the forces. The phenomenological effective forces are supposed to be valid all over the Nuclide Chart and are also supposed to contain all the ingredients needed to describe well low energy nuclear structure phenomena. In addition, the effectives forces are defined over the whole configuration space (in principle over the whole Hilbert space, including even continuum states) and therefore there is no need to specify which orbitals will play a role when a new phenomenon has to be described as all of them enter the game and its role will be determined by the optimization of the energy. As a bonus, no effective charges are needed in the calculation of transition probabilities. Another important advantage of the method comes from the fact that the starting point is always the mean field and therefore the results are much easier to interpret in terms of familiar quantities. Up to now the whole AMPGCM has been performed with the quadrupole moment and restricted to the axially symmetric case, which hints to the computational drawbacks of the method. In principle one would like to take as many generator coordinates as possible, however for the nowadays computers a two dimensional AMPGCM sets the limits of reasonable calculations. The reason is that the effective forces are defined in the whole configuration space. As a consequence, it is capital for the method to perform reasonably well to have a good guess of the relevant degrees of freedom to describe a given phenomenon. Global properties as binding energies, quadrupole moments, etc, as well as ground and collective excited states are usually very well described by the method. However, a very accurate description of any general excited states beyond the AMPGCM in its present form.

In the following we will discuss AMPGCM with effective forces of the Skyrme and Gogny type. In Sect. 2 the mean field approach will be briefly reviewed and the Skyrme and Gogny forces introduced. In Sect. 3 the technicalities of AMP will be discussed and some examples will be used to illustrate the procedure. In Sect. 4 configuration mixing with AMP will be presented an its main outcomes will be discussed with an example. In Sect. 5 an account of the most remarkable results obtained so far with both the Skyrme and Gogny interactions will be presented and briefly discussed. In Sect. 6 we will end up with an outlook of the results discussed and we will discuss further developments of the theory.

2 Symmetry Breaking Mean Field

The mean field HFB wave functions are determined in terms of quasi-particle creation α_μ^+ and annihilation $\alpha_\mu = \left(\alpha_\mu^+\right)^+$ operators (Bogoliubov canonical transformation)

$$\alpha_\mu^+ = \sum_k U_{k\mu} c_k^+ + V_{k\mu} c_k$$

what are given as linear combinations with the amplitudes $U_{k\mu}$ and $V_{k\mu}$ of convenient creation and annihilation single particle operators $c_k^+$and c_k (usually creating or annihilating Harmonic Oscillator eigenstates). The ground state wave function is the product wave function defined by the condition $\alpha_\mu|\varphi\rangle = 0$ and given by

$$|\varphi\rangle = \prod_\mu \alpha_\mu |0\rangle$$

where $|0\rangle$ is the true vacuum wave function and the product runs over all quasi-particle quantum numbers leading to a non zero wave function $|\varphi\rangle$. The $U_{k\mu}$ and $V_{k\mu}$ amplitudes are determined by requiring the HFB energy to be a minimum what leads to the well known HFB equation

$$\begin{pmatrix} h & \Delta \\ -\Delta^* & -h^* \end{pmatrix} \begin{pmatrix} U & V^* \\ V & U^* \end{pmatrix} = \begin{pmatrix} U & V^* \\ V & U^* \end{pmatrix} \begin{pmatrix} E & 0 \\ 0 & -E \end{pmatrix} \tag{1}$$

This is a non linear equation as the HFB fields h and Δ depend on the solution through the density matrix and pairing tensor (see [2, 3, 4, 1] for technical details on how to solve this equation). As was already mentioned in Sect. 1 the solution of (1) does not preserve in many cases the symmetries of the Hamiltonian and is very usual to find that it breaks rotational invariance leading to a deformed matter density distribution which is characterized by its multipole moments like the quadrupole moments $q_{2\mu}$, the octupole ones $q_{3\mu}$, the hexadecapole ones $q_{4\mu}$, etc. In order to better characterize the symmetry breaking solution it turns out to be convenient to study the HFB energy in the neighborhood of the self consistent minimum. In this way we can study whether the solution corresponds to a well developed minimum or if there are other local minima around at an energy relatively close the one found indicating thereby that the mean field solution obtained has got chances of being unstable when additional correlations are included. The best way to do such an study is to carry out constrained calculations where the minimum of the HFB energy is sought but with the constraint that the mean values of relevant operators take a give value. In the case at hand, it is customary to constraint in the mean value of the mass quadrupole operator. The constrained HFB equation is the same as the unconstrained one except for the substitution $h \to h - \lambda o$ where o stands for the matrix of the single particle matrix elements of the constraining operator and λ for the chemical potential that is determined as a Lagrange multiplier to force the solution to satisfy the imposed constraint.

For the interaction to be used in the HFB calculation there are several possible choices but nowadays the most popular options seem to be the effective density dependent interactions of Skyrme or Gogny type. Both are very similar in structure the only difference being that the former is a zero range force contrary to the latter and therefore it cannot be used for the calculation of the matrix elements entering into the definition of the pairing field.

Both the Skyrme [13, 14, 15] and Gogny [16] interactions are two body, density dependent phenomenological interaction given by the sum of four terms

$$v(1,2) = v_C + v_{LS} + v_{DD} + v_{\mathrm{Coul}}.$$

The Coulomb field $v_{\mathrm{Coul}} = e^2/|\boldsymbol{r}_1 - \boldsymbol{r}_2|$, the density dependent interaction $v_{DD} = t_3(1 + P_\sigma x_0)\delta(\boldsymbol{r}_1 - \boldsymbol{r}_2)\rho^\alpha((\boldsymbol{r}_1 + \boldsymbol{r}_2)/2)$, and the two body, non-relativistic spin orbit potential $v_{LS} = iW_{LS}(\boldsymbol{\nabla}_{12}\delta(\boldsymbol{r}_1 - \boldsymbol{r}_2) \wedge \boldsymbol{\nabla}_{12})(\boldsymbol{\sigma}_1 + \boldsymbol{\sigma}_2)$ are the same or very similar in both interactions (they usually differ in the power α entering the density dependent term). However, the central potential v_C is different in both interactions being of zero range in the case of the Skyrme interaction

$$\begin{aligned} v_C(\mathrm{Skyrme}) = {} & t_0(1 + x_0 P_\sigma)\delta(\boldsymbol{r}_1 - \boldsymbol{r}_2) \\ & + \frac{1}{2} t_1(1 + x_1 P_\sigma)[\boldsymbol{k'}^2_{12}\delta(\boldsymbol{r}_1 - \boldsymbol{r}_2) + \delta(\boldsymbol{r}_1 - \boldsymbol{r}_2)\boldsymbol{k}^2_{12}] \\ & + t_2(1 + x_2 P_\sigma)\boldsymbol{k'}^2_{12}\delta(\boldsymbol{r}_1 - \boldsymbol{r}_2)\boldsymbol{k}^2_{12} \end{aligned}$$

whereas it is of **finite range** in the case of the Gogny interaction

$$v_C(\mathrm{Gogny}) = \sum_{i=1,2} e^{-(\boldsymbol{r}_1 - \boldsymbol{r}_2)^2/\mu_i^2} \left(W_i + B_i P_\sigma - H_i P_\tau - M_i P_\sigma P_\tau\right).$$

Both contain the usual combinations of spin and isospin projector operators P_σ and P_τ. In the case of Gogny the finite range is modeled by the sum of two Gaussian of different ranges. The finite range was introduced to prevent the ultraviolet catastrophe that shows up in the evaluation of the pairing potential. As a consequence, it can be used for both the particle-hole and particle-particle channel of the HFB equations. This is not the case for the Skyrme interaction and extra pairing interactions with their corresponding parameters are usually introduced to deal with the particle-particle channel. Concerning the parametrizations of the force, in the case of Skyrme there are over a hundred parameterizations (like SIII[17], SkM[18], SkM* [19] or the Lyon forces [20, 21]) that more or less yield the same bulk nuclear properties at the saturation density but differ in other aspects like their behavior in infinite nuclear and/or neutron matter or their performance to describe the collective response of the nucleus. For the Gogny interaction there are very few parametrizations and in most calculations only the so called D1S is used. It was adjusted back in 1984 [22] to reproduce nuclear matter properties as well as bulk properties of some selected finite nuclei. As this parameterization has performed rather well in all the cases where it has been applied it has been kept over the years. However, taking into account the poor performance of Gogny for neutron matter a new parameterization was proposed [23] but it has not thoroughly been tested up to now. A recent review on the mean field properties of effective density dependent interactions like the ones discussed here can be found in [1].

Since we are focusing in this lecture on the rotational symmetry breaking mechanism, which is mainly characterized by the mass quadrupole moment of the density distribution, the starting point of the calculations (both with the Skyrme or Gogny interaction) is a constrained HFB calculation with the mass quadrupole components as constrained quantities. As the resulting wave functions will be used in the context of Angular Momentum Projection, which represents a very tough computational problem, the calculations will be restricted to axially symmetric, parity conserving configurations denoted by $|\varphi(q_{20})\rangle$ (i.e. by construction only the $\mu = 0$ component of the quadrupole tensor can be different from zero). These HFB wave functions are obtained as a solution of the corresponding HFB equation with the constraint in the mean value of the $\mu = 0$ mass quadrupole operator $\langle\varphi(q_{20})|\, z^2 - 1/2(x^2 + y^2)\,|\varphi(q_{20})\rangle = q_{20}$. Also in both kind of calculations it is customary to neglect the contributions of the Coulomb field to the exchange and pairing potentials due to the high computational cost associated with the calculation of those fields (see [24] for a thorough discussion of these contributions). In the case of the Gogny force calculations we have added the exchange Coulomb energy evaluated in the Slater approximation at the end of the calculation in a perturbative fashion.

Usually the HFB equation is solved for the Skyrme interaction in coordinate space representation by introducing a Cartesian mesh whereas in the case of the Gogny force a Harmonic Oscillator (HO) basis is used including up to N_0 complete shells. The HO length parameters are chosen to be equal in order to preserve the rotational invariance of the basis which is a very important requirement for the subsequent Angular Momentum Projection calculations [25].

As an example of the kind of results it is possible to obtain we have plotted in Fig. 1 the HFB energies computed with the Gogny force as a function of $q = q_{20}/A^{5/3}$ (the variable q is defined to be independent of mass number A, like the deformation parameter β) for five representative nuclei, namely ^{32}Mg, ^{32}S, ^{164}Er, ^{186}Pb and ^{208}Pb. These nuclei have been chosen as they represent typical cases: In the doubly magic ^{208}Pb there is no spontaneous symmetry breaking and the energy has a minimum at $q = 0$ with a very deep and stiff well. In the nucleus ^{164}Er we have two minima one prolate ($q > 0$) which is the absolute minimum and the other oblate ($q < 0$) separated by a rather high barrier. In the nucleus ^{32}S we have an spherical minimum but at a given deformation an excited local minimum appears corresponding to a super-deformed configuration (obviously there are better examples of super-

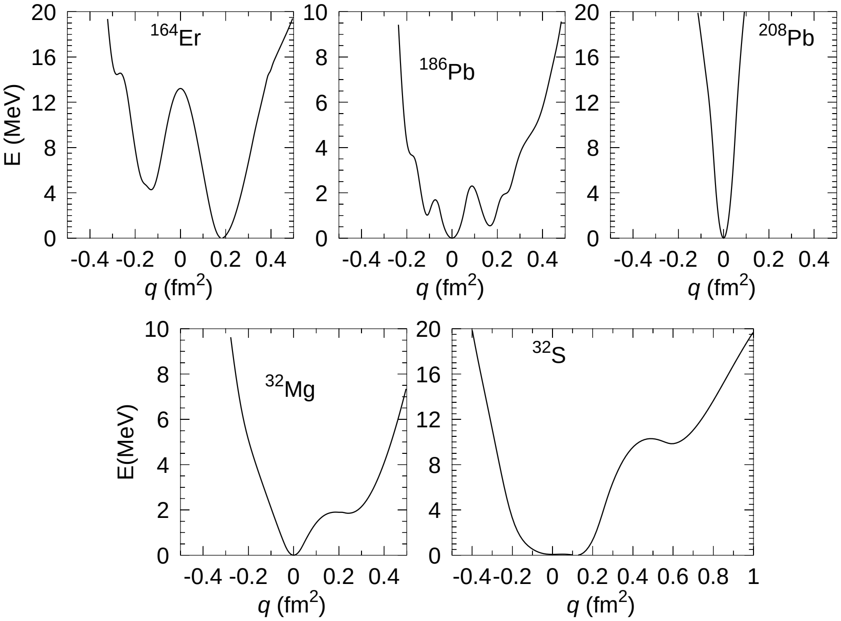

Fig. 1. HFB energies as a function of the quadrupole deformation parameter $q = q_{20}/A^{5/3}$ for five relevant nuclei. Energies are relative to the respective absolute minimum

deformed states both in the rare earth region as well as in the Hg region; we have chosen this particular example as is the only one where subsequent AMP calculations have been carried out). In the case of the neutron deficient magic ^{186}Pb we have three minima one spherical (the absolute minimum) and two excited minima, one prolate and the other oblate, which have energies very close to the one of the ground state (shape coexistence). Finally, in the neutron rich $N = 20$ magic nucleus ^{32}Mg we obtain a spherical minimum ($q = 0$) and a shoulder at around 1 MeV excitation energy. Similar results are obtained for the Skyrme interaction as we will see in Sect. 5.

3 Angular Momentum Projection

In the following subsections we will introduce all the technology to carry out angular momentum projection without entering into much details as most of them can be found in the literature. However, we will devote some more attention to the issue of how to deal with density dependent interactions.

3.1 The Projector Operator

Wave functions $\mid \Psi_{IM}\rangle$ eigenstates of J^2 and J_z with eigenvalues $\hbar^2 I(I+1)$ and $\hbar M$ respectively can be built out of a given deformed mean field state $\mid \varphi\rangle$ by applying the angular momentum projector

$$\mid \Psi_{IM}\rangle = \sum_K g^I_K \hat{P}^I_{MK} \mid \varphi\rangle. \tag{2}$$

The angular momentum projection operator $\hat{P}^I_{MK}$ is given by [5]

$$\hat{P}^I_{MK} = \frac{2I+1}{8\pi^2} \int d\Omega \mathcal{D}^{I*}_{MK}(\Omega) \hat{R}(\Omega) \tag{3}$$

where Ω represents the set of the three Euler angles (α, β, γ), $\mathcal{D}^I_{MK}(\Omega)$ are the well known Wigner functions [26] and $\hat{R}(\Omega) = e^{-i\alpha \hat{J}_z} e^{-i\beta \hat{J}_y} e^{-i\gamma \hat{J}_z}$ is the rotation operator. That $\mid \Psi_{IM}\rangle$ is an angular momentum eigenstate is very easy to check. Applying the rotation operator $\hat{R}(\Omega)$ to it we obtain

$$\hat{R}(\Omega) \mid \Psi_{IM}\rangle = \frac{2I+1}{8\pi^2} \sum_K g^I_K \int d\Omega' \mathcal{D}^{I*}_{MK}(\Omega') \hat{R}(\Omega + \Omega') \mid \varphi\rangle \,.$$

Now the integral on the three Euler angles is rewritten as

$$\int d\Omega' \mathcal{D}^{I*}_{MK}(\Omega' - \Omega) \hat{R}(\Omega') \mid \varphi\rangle = \sum_L \mathcal{D}^I_{ML}(\Omega) \int d\Omega' \mathcal{D}^{I*}_{LK}(\Omega') \hat{R}(\Omega') \mid \varphi\rangle$$

which shows that

$$\hat{R}(\Omega) \mid \Psi_{IM}\rangle = \sum_L \mathcal{D}^I_{ML}(\Omega) \mid \Psi_{IL}\rangle$$

The quantities g^I_K are arbitrary at this point and are usually determined in a variational sense to yield a minimum of the projected energy. The resulting equation will be discussed in the next subsection. Other relevant properties of the projection operator can be easily deduced from the following representation of the projector [27]

$$P^I_{MK} = \sum_\alpha |\alpha IM\rangle\langle\alpha IK| \,. \tag{4}$$

Using this representation is very easy to derive the property

$$\left(P^I_{MK}\right)^+ P^{I'}_{M'K'} = \delta_{II'} \delta_{MM'} P^I_{KK'} \tag{5}$$

as well as

$$\left(P^I_{MK}\right)^+ = P^I_{KM}\,. \tag{6}$$

An interesting quantity is the overlap between the intrinsic wave function $|\varphi\rangle$ and the projected wave functions $\mid \Psi_{IM}\rangle$ that gives the probability amplitude of finding the angular momentum I and third component M in the intrinsic wave function. In Fig. 2 we have plotted such quantities as a function of the quadrupole deformation for the axially symmetric HFB solutions obtained for the nuclei ^{32}Mg and ^{164}Er that were discussed in Sect. 2. As the intrinsic wave functions are axially symmetric the only meaningful quantity in this case is $\mathcal{N}^I(q_{20}) = \langle\varphi(q_{20})|P^I_{00}|\varphi(q_{20})\rangle$ that is the quantity plotted. We observe that the spherical solution ($q_{20} = 0$) only has $I = 0$ component or in other words the HFB solution corresponding to $q_{20} = 0$ is already an eigenstate of angular momentum with $I = 0$. For increasing deformation the $I = 0$ probability decreases whereas the other components increase up to a given point and from there on they decrease. Finally, for large deformations all the components are of the same order of magnitude implying a strong spreading of angular momentum for the intrinsic state.

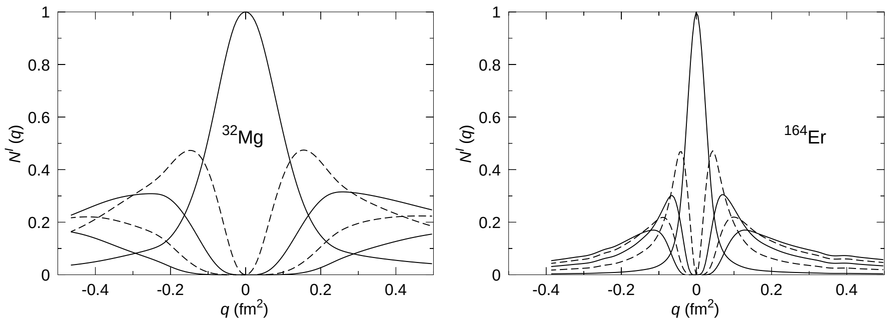

Fig. 2. Projected norms $\mathcal{N}^I(q)$ for $I = 0$, 2, 4, 6 and 8 (dashed lines correspond to $I = 2$ and 6) plotted as a function of the quadrupole deformation parameter $q = q_{20}/A^{5/3}$ for ^{32}Mg and ^{164}Er

Finally, it has to be mentioned that there are other representations of the projector P^I_{MK} as the one of [28] that use the rotation operator in the form $\hat{R}(\kappa) = \exp(-i\kappa\boldsymbol{nJ})$.

3.2 The Projected Energy

The projected energy E^I is simply given by

$$E^I = \frac{\langle\Psi_{IM} \mid \hat{H} \mid \Psi_{IM}\rangle}{\langle\Psi_{IM} \mid \Psi_{IM}\rangle} \tag{7}$$

and the fact that this quantity is independent of M is a direct consequence of the invariance of the Hamiltonian under rotations.

Up to now nothing has been said about the g^I_K coefficients as the geometrical properties of $|\ \Psi_{IM}\rangle$ do not depend on them. However, we can exploit this degree of freedom in a variational sense to minimize the projected energy with respect to those parameters. The resulting equation reads

$$\sum_{K'} g^I_{K'} \left(\langle\varphi|\hat{H}P^I_{KK'}|\varphi\rangle - E^I \langle\varphi|P^I_{KK'}|\varphi\rangle \right) = 0\,.$$

To compute $\langle\varphi|\hat{H}P^I_{KK'}|\varphi\rangle$ we have to perform a three dimensional integral over the Euler angles of an integrand that involves the well known Wigner functions and the Hamiltonian overlap $\langle\varphi|\hat{H}\hat{R}(\Omega)|\varphi\rangle$. The latter quantity can be straightforwardly evaluated by means of the extended Wick theorem [29] and the sign problem of the norm dealt with as suggested in [30], but it turns out that its evaluation for the case at hand is a very intensive computational task that has to be repeated for all the Euler angle mesh points used to evaluate the three dimensional integral numerically. For present single CPU computers this is a task that demands of the order of tens of hours to complete. However, for the Skyrme interaction there has been an attempt [31] to carry out the full calculation for low spins by restricting the number of mesh points in the α and γ integrations and this is a path worth to be explored in the future. For the other approaches mentioned in the introduction the computational cost is much smaller due to the restricted configuration spaces and therefore the full projection is routinely carried out. Fortunately, in many cases the restriction to axially symmetric intrinsic wave functions seems to be a sound approximation [32] that reduces the computational burden by almost two orders of magnitude. For even-even nuclei when $|\varphi\rangle$ is axially symmetric it satisfies $J_z|\varphi\rangle = 0$ and therefore $\langle\varphi|\hat{H}\hat{R}(\Omega)|\varphi\rangle$ reduces to $\langle\varphi|\hat{H}e^{-i\beta J_y}|\varphi\rangle$ which is independent of α and γ. As a consequence the integrals in α and γ are trivial and yields $(2\pi)^2\delta_{K,0}\delta_{K',0}$. With this restriction we get for the projected energy

$$E^I = \frac{\int_0^\pi d\beta \sin(\beta) d^I_{00}(\beta) \langle\varphi|\hat{H}e^{-i\beta J_y}|\varphi\rangle}{\int_0^\pi d\beta \sin(\beta) d^I_{00}(\beta) \langle\varphi|e^{-i\beta J_y}|\varphi\rangle} = \frac{\int_0^\pi d\beta \sin(\beta) d^I_{00}(\beta) h(\beta) n(\beta)}{\int_0^\pi d\beta \sin(\beta) d^I_{00}(\beta) n(\beta)} \quad (8)$$

with $n(\beta) = \langle\varphi|e^{-i\beta J_y}|\varphi\rangle$ and $h(\beta) = \langle\varphi|He^{-i\beta J_y}|\varphi\rangle$. Using as self-consistent symmetry for the intrinsic wave function the signature (essentially the inversion of the x axis, and given by the operator $\Pi e^{-i\pi J_x}$) it is possible to reduce the integration interval to $[0, \pi/2]$ and to show that for even-even nuclei the projected energy is only defined for even values of the angular momentum I when the intrinsic state is reflection symmetric. When the intrinsic state is not reflection symmetric the reduction of the interval of integration implies a projection onto good parity π in addition to the angular momentum projection and the rule $(-1)^I = \pi$ is obtained.

3.3 How to Deal with the Density Dependent Term of the Interactions

When dealing with density dependent (DD) forces we face the problem that the DD term is only defined at the mean field level: In the evaluation of the expectation value of the Hamiltonian $\langle\varphi|\hat{H}|\varphi\rangle$ the DD interaction is given in terms of $\rho(\boldsymbol{R}) = \langle\varphi|\hat{\rho}(\boldsymbol{R})|\varphi\rangle$ which is evaluated as an expectation value with the **same** wave function used in the evaluation of the energy. However, in the calculation of the projected energies we need the Hamiltonian overlap $\langle\varphi|\hat{H}\hat{R}(\Omega)|\varphi\rangle$ and, as the DD term has a phenomenological origin, it is not clear which density should be used in the DD term of the interaction for the evaluation of the above mentioned overlap. The same problem arises with the overlap needed in the Generator Coordinate Method (GCM), namely $\langle\varphi_0|\hat{H}|\varphi_1\rangle$. Several **prescriptions** have been proposed to cope with this problem: in one [33], inspired by a generalized Brueckner expansion, the density is replaced by the linear combination $\frac{1}{2}(\langle\varphi|\hat{\rho}(\boldsymbol{R})|\varphi\rangle + \langle\varphi|\hat{\rho}(\boldsymbol{R})\hat{R}(\Omega)|\varphi\rangle)$; in other called the "mixed density" prescription the quantity $\langle\varphi|\hat{\rho}(\boldsymbol{R})\hat{R}(\Omega)|\varphi\rangle/\langle\varphi|\hat{R}(\Omega)|\varphi\rangle$ is proposed [34] (see also [35] for a thorough discussion in the context of Particle Number Projection) and it is inspired by the way the Hamiltonian overlap is computed with the aid of the extended Wick theorem. There are some more prescriptions, like the one proposing a rotational invariant density dependent term, but we will not comment them here. In any case, as in most of the prescriptions the DD term breaks rotational invariance and even hermiticity, it is very important to show that the prescriptions are consistent with general properties of the projected energy like being a real quantity and that the projected energy is independent of M, i.e., Eq. (7) is satisfied. In [36] has been shown that the "mixed density" prescription $\langle\varphi|\hat{\rho}(\boldsymbol{R})\hat{R}(\Omega)|\varphi\rangle/\langle\varphi|\hat{R}(\Omega)|\varphi\rangle$ satisfies the two previous requirements as it also does the other prescription. At this point it might seem paradoxical to have a Hamiltonian which is not rotational invariant but this apparent paradox can be solved if density dependent Hamiltonian are thought not as genuine Hamiltonian but rather as devices (in the spirit of the Density Functional Theory) to get an elaborated energy functional of the density.

3.4 Transition Probabilities and Spectroscopic Factors

Transition probabilities are the physical quantities that have most sensitivity to the approximations made to the wave functions. For instance, transition probabilities have selection rules that can not be reproduced unless the wave functions used are eigenstates of the angular momentum Casimir operators J^2 and J_z. In this section we will present the way they are computed when the wave functions used come from an angular momentum projected intrinsic state and specialized formulas for the case of an axially symmetric intrinsic state will be presented.

The only property we will need is the transformation law of the multipole operators $\hat{Q}_{\lambda\mu}$ under rotations

$$\hat{R}(\Omega)\hat{Q}_{\lambda\mu}\hat{R}^{\dagger}(\Omega) = \sum_{\mu'} \mathcal{D}^{\lambda}_{\mu'\,\mu}(\Omega)\hat{Q}_{\lambda\mu'} \tag{9}$$

Using the well known result for the product of two Wigner functions [26] as well as the definition of (3) for the angular momentum projection operator and the property

$$\hat{P}^{I}_{MK}\hat{P}^{I'}_{K'M'} = \delta_{I,I'}\delta_{K,K'}\hat{P}^{I}_{MM'} \tag{10}$$

we obtain after some algebra the result

$$\begin{aligned}\hat{P}^{I_f}_{K_f M_f}\hat{Q}_{\lambda\mu}\hat{P}^{I_i}_{M_i K_i} &= \langle I_i M_i \lambda\mu \mid I_f M_f\rangle \\ &\quad\times \sum_{\nu\mu'} (-)^{\mu'-\mu}\langle I_i \nu \lambda\mu' \mid I_f K_f\rangle \hat{Q}_{\lambda\mu'}\hat{P}^{I_i}_{\nu K_i}\,. \end{aligned}\tag{11}$$

With the definition of the projected wave functions (2) and the previous result we obtain

$$\langle \Psi_{I_f M_f} \mid \hat{Q}_{\lambda\mu} \mid \Psi_{I_i M_i}\rangle = \frac{\langle I_i M_i \lambda\mu \mid I_f M_f\rangle}{\sqrt{2I_f+1}}\langle I_f \mid\mid \hat{Q}_{\lambda} \mid\mid I_i\rangle \tag{12}$$

with

$$\begin{aligned}\langle I_f \mid\mid \hat{Q}_{\lambda} \mid\mid I_i\rangle &= \frac{(2I_i+1)(2I_f+1)}{8\pi^2}(-)^{I_i-\lambda}\sum_{K_i K_f \nu\mu'}(-)^{K_f} g^{I_f *}_{K_f} g^{I_i}_{K_i} \\ &\quad\times \begin{pmatrix} I_i & \lambda & I_f \\ \nu & \mu' & -K_f \end{pmatrix} \int d\Omega\, \mathcal{D}^{I_i *}_{\nu K_i}(\Omega)\langle \varphi_f \mid \hat{Q}_{\lambda\mu'}\hat{R}(\Omega) \mid \varphi_i\rangle\,. \end{aligned}\tag{13}$$

The previous derivation only uses the tensor properties of the electric multipole operator and therefore also applies to the case of the magnetic multipole operators.

Taking advantage of the axial symmetry of the intrinsic wave function as well as the self-consistent symmetry $\Pi e^{-i\pi\hat{J}_x}$ we can simplify the above expressions as follows. First we have

$$\langle \varphi_f \mid \hat{Q}_{\lambda\mu'}\hat{R}(\Omega) \mid \varphi_i\rangle = e^{i\alpha\mu'}\langle \varphi_f \mid \hat{Q}_{\lambda\mu'} e^{-i\beta\hat{J}_y} \mid \varphi_i\rangle \tag{14}$$

that leads to

$$\begin{aligned}&\textstyle\int d\Omega\, \mathcal{D}^{I_i *}_{QK_i}(\Omega)\langle \varphi_f \mid \hat{Q}_{\lambda\mu'}\hat{R}(\Omega) \mid \varphi_i\rangle = 4\pi^2 \delta_{Q-\mu'}\delta_{K_i 0} \\ &\quad\times \textstyle\int_0^{\pi} d\beta \sin(\beta) d^{I_i *}_{-\mu' 0}(\beta)\langle \varphi_f \mid \hat{Q}_{\lambda\mu'} e^{-i\beta\hat{J}_y} \mid \varphi_f\rangle\,. \end{aligned}\tag{15}$$

Applying this result to the expression (13) we obtain

$$\begin{aligned}
\langle I_f \mid\mid \hat{Q}_\lambda \mid\mid I_i \rangle &= \frac{(2I_i+1)(2I_f+1)}{2}(-)^{I_i-\lambda} \sum_{\mu'} \begin{pmatrix} I_i & \lambda & I_f \\ -\mu' & \mu' & 0 \end{pmatrix} \\
&\times \int_0^{\pi} d\beta \sin(\beta) d^{I_i *}_{-\mu' 0}(\beta) \langle \varphi_f \mid \hat{Q}_{\lambda\mu'} e^{-i\beta \hat{J}_y} \mid \varphi_i \rangle \\
&= (2I_i+1)(2I_f+1)(-)^{I_i-\lambda} \frac{1+(-)^{I_i}}{2} \sum_{\mu'} \begin{pmatrix} I_i & \lambda & I_f \\ -\mu' & \mu' & 0 \end{pmatrix} \\
&\times \int_0^{\frac{\pi}{2}} d\beta \sin(\beta) d^{I_i *}_{-\mu' 0}(\beta) \langle \varphi_f \mid \hat{Q}_{\lambda\mu'} e^{-i\beta \hat{J}_y} \mid \varphi_i \rangle \qquad (16)
\end{aligned}$$

where we have reduced, in the last line, the integration interval to half the original one making use of the self-consistent signature symmetry of the intrinsic wave function.

3.5 Variation Before and After Projection

Now that we know how to compute the projected quantities we can take for a given nucleus its mean field ground state and project it out to obtain the projected energies for different angular momenta. This procedure is called the Projection After Variation (PAV) method as the intrinsic state is determined at the mean field level and projected afterwards. For the nuclei used as examples in Sect. 1 we will obtain for the $I = 0$ ground state the same projected energy as the intrinsic one for all the examples discussed except for ^{164}Er where a lowering of 3.07 MeV is obtained. For $I = 2$ the projected energy for those nuclei with an spherical intrinsic state is an indeterminacy of the type zero divided by zero. For the deformed ^{164}Er we will obtain for $I = 2$ an excited state which is 139.4 keV higher than the $I = 0$ projected ground state.

As the energy gain due to projection for the ground state of ^{164}Er was of the order of a few MeV one may wonder whether this energy gain can be strong enough for some deformed configurations as to overcome the mean field energy differences and produce projected energies which could be lower than the one given by the PAV method. To elucidate this possibility we have plotted in Fig. 3 the $I = 0$ and $I = 2$ projected energies along with the HFB results (dashed line) for all the nuclei considered in Sect. 2.

For the well deformed ^{164}Er nucleus the effect of projection is just an overall shift of the energy with respect to the HFB curve except around $q = 0$ where for $I = 0$ the projected energy has to coincide with the intrinsic one. In this nucleus the $I = 2$ curve is so close to the $I = 0$ one that is almost indistinguishable from the latter with the scale used for the plot, except around $q = 0$ where the intrinsic wave function has an overlap zero with the $I = 2$ projected state (see Fig. 2).

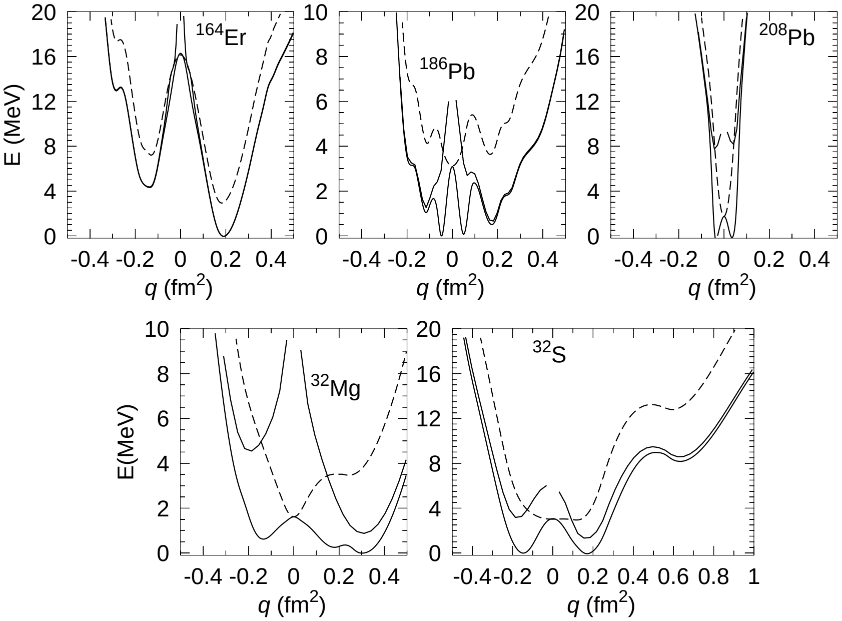

Fig. 3. Angular momentum projected energies for $I = 0$ and $I = 2$ along with the HFB energy (dashed curves) plotted as a function of the quadrupole deformation parameter $q = q_{20}/A^{5/3}$ for five relevant nuclei.

Not surprisingly the projected energies show minima in all nuclei considered (except ^{164}Er) which correspond to deformed intrinsic configurations ! In addition, the intrinsic configurations corresponding to the $I = 0$ and $I = 2$ minima are in the examples presented very close but they do not share exactly the same intrinsic state. If we now take as the wave function of the system for each angular momentum I the one that gives the lower projected energy as a function of q we will be doing things properly (the variational principle again) and we will be using a restricted version of the Projection Before Variation method (PBV). In the PBV method the intrinsic wave function for each angular momentum is determined by minimizing not the intrinsic energy but the projected one. The example mentioned above is a restricted version of the PBV method as we are not exploring, by considering only wave functions constrained to a given quadrupole deformation, the whole Hilbert space. However, we can argue that as the quadrupole moment is the main quantity characterizing the amount of rotational symmetry breaking, it is the most relevant degree of freedom in terms of the PBV method and therefore just considering it gives results very close to the ones of the exact PBV procedure.

At this point it has to be said that except the shell model, all the techniques mentioned in the introduction aiming to a better description of the nuclear many body problem are different versions (or views) of the PBV method. What is different among them is the way the Hilbert space is searched (fully in the Tubingen approach, by means of multiquasiparticle excited states in the PSM, stochastically in the MCSM, etc).

Coming back to the discussion of Fig. 3 it is amazing the large effect caused by projection for the $I = 0$ ground state even in spherical nuclei ! The two light nuclei ^{32}Mg and ^{32}S become well deformed when projection is considered (in good agreement with the experimental results for ^{32}Mg). Even the double magic nucleus ^{208}Pb becomes slightly deformed[1] and in this way it gains 1.8 MeV in correlation energy. This is an important fact (also observed in other doubly magic nuclei like ^{16}O, ^{40}Ca and ^{48}Ca) that should be taken into account in the fitting procedure of the effective interactions treated in this paper. In this respect, the effect can also be relevant for the evaluation of masses with astrophysical purposes: in a recent fit of the Skyrme interaction [37] to the known nuclear masses the rotational energy correction is included (in an approximate way to be discussed below) for deformed nuclei in the spirit of the PAV and therefore is disregarded for spherical nuclei. However, taking into account the results just discussed for ^{208}Pb the rotational energy correction should also be considered for spherical nuclei although the procedure to evaluation this quantity can be much more cumbersome than for the situation of a well deformed ground state.

The important quantity in the description of the ground state in the context of the PBV method is the ground state energy gain due to the projection and given for even-even nuclei by

$$E_{REC} = E_{HFB} - E^{I=0} \tag{17}$$

It is also called the Rotational Energy Correction (REC) and is a quantity which increases with increasing deformation of the system and its typical values are in the range of a few MeV. This is an important correction when shape coexistence is present in the system as it can substantially modify the picture emerging from the mean field and make an excited minimum or shoulder the ground state. It also reduces in a few MeV the fission barrier heights with respect to the mean field result and can have important effects even for spherical nuclei. Several examples will be discussed below in Fig. 6.

---

[1] In fact there are two deformed minima, one prolate and the other oblate with approximately the same energy and the same absolute value of the quadrupole moment. In these cases as we will see in Section 4 one should perform configuration mixing calculations. The resulting wave function provides an spherical nucleus and an additional energy lowering of about 1 MeV

3.6 An Approximate Evaluation of the Projected Energies: The Strong Deformation Limit, the Kamlah Expansion and the Like

The exact expressions for the projected energy and transition probabilities are too complicated to have an intuitive understanding of their effects. Therefore it is convenient to have estimations given in terms of simple quantities expressible in terms of the underlying intrinsic state. On the other hand, the evaluation of the exact projected quantities is rather costly in terms of computational time an is desirable to have good estimations that are easier to compute. Such estimations can be easily obtained by means of the Kamlah expansion [38, 39] which is valid in the strong deformation limit. To understand the essence of the approximation let us consider for simplicity the axially symmetric case and angular momentum zero. The projected energy is given in this situation by

$$E^{I=0}=\frac{\int_0^{\pi/2}d\beta\sin(\beta)h(\beta)n(\beta)}{\int_0^{\pi/2}d\beta\sin(\beta)n(\beta)}$$

where, as compared to (8) we have reduced the integration interval to $\pi/2$ by using the signature as a symmetry of the intrinsic wave function. If the intrinsic wave function is strongly deformed, the overlap $n(\beta)$ will only be significantly different from zero when $\beta\approx 0$ and will experience a fast decay away from that value. In fact, $n(\beta)$ can be approximated by [3]

$$n(\beta)\approx e^{-\frac{1}{2}\langle J_y^2\rangle\beta^2}\,. \tag{18}$$

Next, we assume that $h(\beta)$ is a smooth function of β that can be expanded to a good accuracy in a power series up to second order in β

$$h(\beta)\approx h_0-\frac{1}{2}h_2\beta^2+\ldots \tag{19}$$

with $h_0=\langle H\rangle$ and $h_2=-\frac{d^2h(\beta)}{d\beta^2}_{|\beta=0}$. Then the projected energy is given by

$$E^{I=0}=h_0-\frac{1}{2}h_2\Lambda_0(\langle J_y^2\rangle)$$

where $\Lambda_0(\langle J_y^2\rangle)=\frac{\int_0^{\pi/2}d\beta\sin(\beta)\beta^2e^{-\frac{1}{2}\langle J_y^2\rangle\beta^2}}{\int_0^{\pi/2}d\beta\sin(\beta)e^{-\frac{1}{2}\langle J_y^2\rangle\beta^2}}$. As this function goes to one when $\langle J_y^2\rangle>>1$ we finally arrive to the well known formula for the rotational energy correction in the strong deformation limit

$$E^{I=0}=h_0-\frac{1}{2}h_2 \tag{20}$$

which is nowadays widely used in many calculations to get an estimation of the effect of angular momentum projection in the $I=0$ ground state. To test the accuracy of this approximation we have computed for the nucleus ^{164}Er the exact quantities $n(\beta)$ and $h(\beta)$ for different quadrupole deformations and the results are presented in Fig. 4 along with the approximate estimates of (18) and (19).

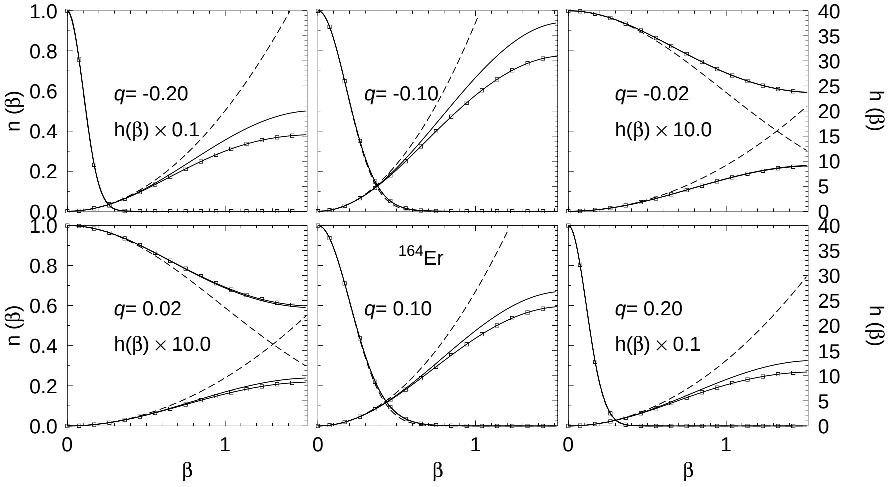

Fig. 4. A comparison of the exact $n(\beta)$ and $h(\beta)$ (full line with symbols) with the approximated expressions of (21) and (22) (full line) as well as the standard ones of (18)and (19) (dashed lines) for different deformation parameters q. The quantity $h(\beta)$ has been multiplied in each panel by the indicated factor

We observe how for strong and moderate deformations the approximated estimates do rather well and we can conclude that the approximation to the $I = 0$ projected energy is reasonable. However, for small deformations this is not the case and we expect a failure of the method. As it was suggested by Reinhard [40, 41, 32] the behavior of the overlaps can be better approximated for the small deformation case by using the ansatz

$$n(\beta) \approx e^{-\frac{1}{2}\langle J_y^2\rangle \sin^2(\beta)} \tag{21}$$

and

$$h(\beta) \approx h_0 - \frac{1}{2} h_2 \sin^2(\beta) + \ldots \tag{22}$$

instead of (18) and (19). This ansatz is inspired by the properties $n(\beta) = n(\pi - \beta)$ and $h(\beta) = h(\pi - \beta)$ that the exact quantities have to satisfy when the simplex symmetry is imposed in the intrinsic wave function and also by analytical results obtained with harmonic oscillator wave functions. To check the quality of the new ansatz we have plotted in Fig. 4 the new quantities.

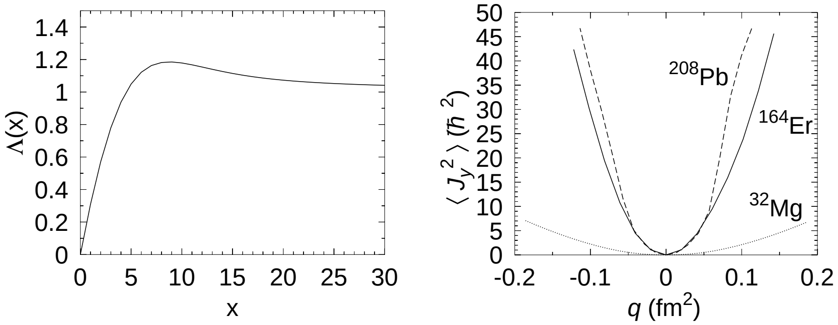

Fig. 5. Left panel: The function $\Lambda(x)$ defined in (24) as a function of x. Right panel: The expectation value $\langle J_y^2 \rangle$ as a function of the deformation parameter q

We observe how the quality of the ansatz is excellent for small deformations and it also improves the results at moderate and strong deformations.

Using the new ansatz, the projected energy for $I = 0$ is now given by

$$E^{I=0} = h_0 - \frac{1}{2} h_2 \Lambda(\langle J_y^2 \rangle) \tag{23}$$

with

$$\Lambda(\langle J_y^2 \rangle) = \frac{\int_0^{\pi/2} d\beta \sin(\beta) \beta^2 e^{-\frac{1}{2}\langle J_y^2 \rangle \sin^2(\beta)}}{\int_0^{\pi/2} d\beta \sin(\beta) e^{-\frac{1}{2}\langle J_y^2 \rangle \sin^2(\beta)}}. \tag{24}$$

To understand the changes induced by the new ansatz the universal function $\Lambda(x)$ has been plotted in the left panel of Fig. 5 as a function of x. There we observe how for big values of x it goes to 1 recovering the standard results and it rapidly decreases for x going to zero in good agreement with the fact that $\langle J_y^2 \rangle = 0$ corresponds (for axially symmetric systems) to an spherical wave function where the effect of angular momentum projection is null. Interestingly, the function $\Lambda(x)$ has a maximum at $x \approx 7$ thus enhancing the rotational energy correction at this point. From the shape of this curve it is clear that $\Lambda(x)$ induces strong changes in the energy for x values smaller than 7 and an smooth modulation of it at larger values. The interesting question is to know the deformation range for which x, i.e., $\langle J_y^2 \rangle$, satisfies $0 \leq \langle J_y^2 \rangle \leq 7$. In the right panel of Fig. 5 we have represented $\langle J_y^2 \rangle$ versus q for the indicated nuclei. We find that the relevant intervals are $-0.2 \leq q \leq 0.2$ for ^{32}Mg and $-0.05 \leq q \leq 0.05$ for ^{164}Er and ^{208}Pb.

In Fig. 6 we now compare the exact rotational energy correction (17) at zero spin with the standard approximation (20) and the one by Reinhard (23) for the mentioned nuclei. The exact REC is zero for spherical intrinsic states, it typically increases rather abruptly for small deformations and at some point it slides down and from there on its growing rate stabilizes to a smaller value. It is interesting to see that the largest changes in the REC are given in the predicted range $-0.2 \leq q \leq 0.2$ for ^{32}Mg and $-0.05 \leq q \leq 0.05$ for ^{164}Er and ^{208}Pb. As can be observed in this plot the standard approximate expression of (20) does pretty bad in the corresponding deformation ranges indicated above while Reinhard's one does pretty well even in the critical regions. This is an encouraging result as it can enormously simplify the estimation of the rotational energy correction in all kind of nuclei, spherical or deformed, and therefore can make possible its use in massive mass evaluations like the ones needed for astrophysical purposes.

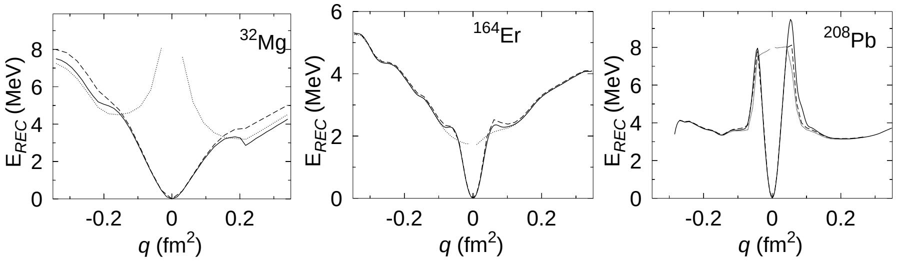

Fig. 6. Rotational energy corrections as a function of the quadrupole deformation parameter $q = q_{20}/A^{5/3}$ for ^{32}Mg, ^{164}Er and ^{208}Pb. The full line represents the exact result of (17) whereas the dashed line stands for the approximation (23) and the dotted one for the standard correction, see (20)

What we have said up to now is based in the assumption that the intrinsic wave function is axially symmetric and we have restricted the discussion to zero spin. In the general case things can be worked out for the full projection [38, 39] and the following expression is obtained in the strong deformation limit

$$\begin{aligned} E^I &= \langle H \rangle - \frac{\langle \Delta \boldsymbol{J}^2 \rangle}{2\mathcal{J}_Y} + \omega \left(\sqrt{I(I+1) - \langle J_z^2 \rangle} - \langle J_x \rangle \right) \\ &\quad + \frac{1}{2\mathcal{J}_Y} \left(\sqrt{I(I+1) - \langle J_z^2 \rangle} - \langle J_x \rangle \right)^2 \end{aligned} \tag{25}$$

where $\mathcal{J}_Y$ is the Yoccoz moment of inertia given by

$$\frac{1}{2\mathcal{J}_Y} = \frac{\langle \Delta H \Delta \boldsymbol{J}^2 \rangle}{2\left(\langle \Delta J_x^2 \rangle^2 + \langle J_y^2 \rangle^2 + \langle J_z^2 \rangle^2 \right)} \tag{26}$$

and

$$\omega = \frac{\langle H \Delta J_x \rangle}{\langle \Delta J_x^2 \rangle} \, . \tag{27}$$

In order to pin down the physics behind this expression let us assume that the intrinsic wave function is time reversal invariant. In this case $\omega = \langle J_x \rangle = 0$.

If, additionally, we impose an axially symmetric wave function then $\langle J_z^2 \rangle = 0$ and the approximate projected energy becomes

$$E^I = \langle H \rangle - \frac{\langle \Delta \boldsymbol{J}^2 \rangle}{2\mathcal{J}_Y} + \frac{I(I+1)}{2\mathcal{J}_Y}$$

which corresponds to the energy of a rotor with intrinsic energy $\langle H \rangle - \frac{\langle \Delta \boldsymbol{J}^2 \rangle}{2\mathcal{J}_Y}$, angular momentum I and moment of inertia $\mathcal{J}_Y$. In other words, we have a rotational band with the typical $I(I+1)$ behavior and with the Yoccoz moment of inertia. The intrinsic energy is not simply $\langle H \rangle$ but it is reduced by the so called rotational energy correction (REC) given by $\frac{\langle \Delta \boldsymbol{J}^2 \rangle}{2\mathcal{J}_Y}$. Unfortunately, in this case the ansatz proposed by Reinhard is not easy to generalize and work is needed in order to get equivalent results in the most general case. In this respected, perhaps the representation of [28] can prove to be useful.

Another interesting aspect of the approximate energy obtained in (25) concerns its use in the context of the Projection Before Variation method. If one assumes that the approximate energy is a sound approximation to the projected energy then, requiring the intrinsic state to lead to a minimum of that expression, is an approximate PBV minimization process. The minimization process gets rather cumbersome due to the rotational energy correction term but it has been shown in many examples that this correction stays rather constant in the domain of validity of (25) and therefore it is safe to neglect it in the variational process. Neglecting the variation of the REC one ends up with the variational equation of the self-consistent cranking model

$$\delta \langle \varphi | H - \omega J_x | \varphi \rangle = 0 \tag{28}$$

where ω is determined as to satisfy the constraint

$$\langle \varphi | J_x | \varphi \rangle = \sqrt{I(I+1) - \langle J_z^2 \rangle}\,.$$

This equation has to be solved for each value of I and the intrinsic wave function is therefore I dependent. Another interesting aspect is related to the fact that J_x is odd under time reversal and therefore the intrinsic wave function breaks time reversal invariance as well as axial symmetry. The energy spectrum obtained is well represented by the energy of a rotor

$$E^I = \frac{I(I+1)}{2\mathcal{J}_{SCC}(I)}$$

where the self-consistent cranking moment of inertia eventually depends on I. If we now compare this spectrum with the one given by (25) corresponding to the PAV method we notice that the two moments of inertia are formally different. In the cranking model we have the self-consistent moment of inertia whereas in the PAV method we have the Yoccoz one. How different they are depends on the interaction (probably on the effective mass but there is no formal proof) but to give a taste of the kind of differences one can expect we can say that in the case of ^{164}Er the energy difference $E^{I=2} - E^{I=0}$ is 139.4 keV for the exact PAV whereas the cranking model gives 78.8 keV, that is the cranking result is roughly a factor 0.6 smaller than the PAV one. Formally, the cranking results are better than the PAV (even though they can compare worse with experiment due to the interaction used) as the former are based on the PBV method. However, this does not mean that we have also to use the self-consistent cranking moment of inertia (or its close cousin, the Thouless Valatin moment of inertia) in the evaluation of the rotational energy correction $E_{REC} = \frac{\langle \Delta \boldsymbol{J}^2 \rangle}{2\mathcal{J}_Y}$ as it is sometimes done: the REC has always to be evaluated with the Yoccoz moment of inertia. The above discussion is also in good agreement with the results of [42, 43] where also an approximate PBV was carried out but in a different context.

4 Configuration mixing

In the previous sections we have had the opportunity to glance to several Angular Momentum Projected Energy Surfaces (AMPES) belonging to different nuclei. In many of them we have obtained several minima which are close in energy and are also separated by low and narrow barriers and therefore it is expected that configurations mixing of those states will lead to a further reduction of the energy of the states. In this section we will investigate this possibility in the framework of the Angular Momentum Projected Generator Coordinate Method (AMPGCM). A general AMPGCM wave function $\mid \Phi_{IM}(\sigma)\rangle$ is written as a linear combination of the "generating" functions $\mid \Psi_{IM}(\mathbf{q})\rangle$ which are obtained by projecting onto good angular momentum a set of intrinsic wave functions which are characterized by several parameter (usually multipole moments of the mass distribution) $\mathbf{q} = \{q_1, q_2, ...\}$. Explicitly we have

$$\mid \Phi_{IM}(\sigma)\rangle = \int d\mathbf{q} f^{I,\sigma}(\mathbf{q}) \mid \Psi_{IM}(\mathbf{q})\rangle = \sum_K \int d\mathbf{q} \overline{f}_K^{I,\sigma}(\mathbf{q}) P^I_{MK} |\varphi(\mathbf{q})\rangle \,. \quad (29)$$

The amplitudes $f^{I,\sigma}(\mathbf{q})$ are solutions of the Hill-Wheller (HW) equation [6]

$$\sum_{K'} \int d\mathbf{q}' \overline{f}_{K'}^{I,\sigma}(\mathbf{q}') \left(\langle \varphi(\mathbf{q}) | H P^I_{KK'} | \varphi(\mathbf{q}') \rangle - E^{I,\sigma} \langle \varphi(\mathbf{q}) | P^I_{KK'} | \varphi(\mathbf{q}') \rangle \right) = 0 \,.$$

This equation is derived by imposing the AMPGCM energy to be a minimum. As it was mentioned before the calculations are usually restricted to axially symmetric ($K = 0$) configurations and in this case the angular momentum projected Hill-Wheeler equation reduces to

$$\int d\mathbf{q}' f^{I,\sigma}(\mathbf{q}') \left(\langle \varphi(\mathbf{q}) | H P^I_{00} | \varphi(\mathbf{q}') \rangle - E^{I,\sigma} \langle \varphi(\mathbf{q}) | P^I_{00} | \varphi(\mathbf{q}') \rangle \right) = 0 \,.$$

This is an integral equation where the Hamiltonian kernel $\mathcal{H}^I(\mathbf{q},\mathbf{q}') = \langle\varphi(\mathbf{q})|HP^I_{00}|\varphi(\mathbf{q}')\rangle$ and the norm overlap $\mathcal{N}^I(\mathbf{q},\mathbf{q}') = \langle\varphi(\mathbf{q})|P^I_{00}|\varphi(\mathbf{q}')\rangle$ play the central role. The HW equation is a non-orthogonal eigenvalue equation that is usually recasted in terms of orthogonal quantities by diagonalizing first the norm overlap

$$\int d\mathbf{q}'\mathcal{N}^I(\mathbf{q},\mathbf{q}')u_l(\mathbf{q}') = n^I_l u_l(\mathbf{q})$$

what allows to write the norm overlap as

$$\mathcal{N}^I(\mathbf{q},\mathbf{q}') = \sum_l n^I_l u^*_l(\mathbf{q})u_l(\mathbf{q}')\,.$$

Inserting this expression into the HW equation and defining the amplitudes

$$g^{I,\sigma}_l = (n^I_l)^{1/2}\int d\mathbf{q}' f^{I,\sigma}(\mathbf{q}')u_l(\mathbf{q}')$$

and using the inverse relation

$$f^{I,\sigma}(\mathbf{q}') = \sum_l \frac{g^{I,\sigma}_l}{(n^I_l)^{1/2}}u^*_l(\mathbf{q}') \tag{30}$$

we end up with the HW equation written as

$$\sum_{l'}(H^C_{ll'} - E^{I,\sigma}\delta_{ll'})g^{I,\sigma}_{l'} = 0$$

where the collective image of the Hamiltonian kernel $H^C_{ll'}$ is defined as

$$H^C_{ll'} = \int d\mathbf{q}d\mathbf{q}'\frac{u^*_l(\mathbf{q})}{(n^I_l)^{1/2}}\mathcal{H}^I(\mathbf{q},\mathbf{q}')\frac{u_{l'}(\mathbf{q}')}{(n^I_{l'})^{1/2}}\,.$$

The solution of this reduced equation produces the eigenvalues $E^{I,\sigma}$ labeled by the σ index and the eigenvectors $g^{I,\sigma}_l$ from which we can compute the amplitudes $f^{I,\sigma}(\mathbf{q}')$ using (30).

In order to interpret the GCM results it is customary to introduce the collective wave functions

$$g^{I,\sigma}(\mathbf{q}) = \int d\mathbf{q}'\left(\mathcal{N}^{1/2}\right)^I(\mathbf{q},\mathbf{q}')f^{I,\sigma}(\mathbf{q}') = \sum_l g^{I,\sigma}_l u_l(\mathbf{q})$$

and the reason is that they are orthogonal, contrary to their counterpart $f^{I,\sigma}(\mathbf{q}')$, and therefore their modulus squared can be interpreted as a probability amplitude.

In our particular case the set of labels $\mathbf{q}$ reduces to the quadrupole moment q_{20}. If we take into account the axial symmetry imposed to the intrinsic wave functions and write explicitly the projector operator we end up with the following expressions for the norm overlap

$$\mathcal{N}^I(q_{20},q_{20}^{'}) = (2I+1)\int_0^{\frac{\pi}{2}} d\beta \sin(\beta) d_{00}^{I*}(\beta)\langle\varphi(q_{20}) \mid e^{-i\beta\hat{J}_y} \mid \varphi(q_{20}^{'})\rangle \tag{31}$$

and the Hamiltonian kernel

$$\mathcal{H}^I(q_{20},q_{20}^{'}) = (2I+1)\int_0^{\frac{\pi}{2}} d\beta \sin(\beta) d_{00}^{I*}(\beta)\langle\varphi(q_{20}) \mid \hat{H}_{DD} e^{-i\beta\hat{J}_y} \mid \varphi(q_{20}^{'})\rangle \tag{32}$$

where $\hat{H}_{DD}$ now depends on the density $\overline{\rho}_\beta^{GCM}(\boldsymbol{r})$ given by

$$\overline{\rho}_\beta^{GCM}(\boldsymbol{R}) = \frac{\langle\varphi(q_{20}) \mid \hat{\rho}(\boldsymbol{R}) e^{-i\beta\hat{J}_y} \mid \varphi(q_{20}^{'})\rangle}{\langle\varphi(q_{20}) \mid e^{-i\beta\hat{J}_y} \mid \varphi(q_{20}^{'})\rangle}\,. \tag{33}$$

This is the obvious generalization in the framework of the configuration mixing calculation of the mixed density prescription described in Sect. 3.3 for the density dependent part of the interaction.

Finally, from the knowledge of the amplitudes $f^{I,\sigma}(q_{20})$, we can compute the reduced $B(E2)$ transition probabilities and the spectroscopic quadrupole moments $Q^{\mathrm{spec}}(I,\sigma)$. This is one of the main motivations for carrying out a configuration mixing calculation of angular momentum projected wave functions in the case of Gogny and Skyrme forces, since both interactions allow the use of full configuration spaces and then one is able to compute transition probabilities and spectroscopic quadrupole moments without effective charges. In the framework of the AMPGCM the $B(E2)$ transition probability between the states (I_i,σ_i) and (I_f,σ_f) is expressed as (see Sect. 3.4 for more details)

$$\begin{aligned} B(E2, I_i\sigma_i \rightarrow I_f\sigma_f) = {} & \frac{e^2}{2I_i+1} \\ & \times \left| \int dq_i dq_f f^{*I_f,\sigma_f}(q_f)\langle I_f q_f \mid\mid \hat{Q}_2 \mid\mid I_i q_i\rangle f^{I_i,\sigma_i}(q_i)\right|^2 \end{aligned} \tag{34}$$

and the spectroscopic quadrupole moment for the state $(I\geq 2,\sigma)$ is given by

$$\begin{aligned} Q^{\mathrm{spec}}(I,\sigma) = {} & e\sqrt{\frac{16\pi}{5}}\begin{pmatrix} I & 2 & I \\ I & 0 & -I \end{pmatrix} \\ & \times \int dq_i dq_f f^{*I,\sigma}(q_f)\langle I q_f \mid\mid \hat{Q}_2 \mid\mid I q_i\rangle f^{I,\sigma}(q_i)\,. \end{aligned} \tag{35}$$

5 Results

In order to illustrate the whole procedure we will discuss now the ^{32}Mg nucleus in detail and at the end we will give an overview of the available results obtained with the Skyrme and Gogny interactions. The nucleus ^{32}Mg is a nice example as it is one of the neutron rich magic (N=20) nuclei where the shell closure is broken. The most convincing experimental evidence for a deformed ground state in the N=20 isotopes is found in the ^{32}Mg nucleus where both the excitation energies of the lowest lying 2^+ [44] and 4^+ [45, 46] states and the $B(E2, 0^+ \rightarrow 2^+)$ transition probability [47] have been measured. The low excitation energy of the 2^+ state, the high value of the $B(E2)$ transition probability and also the ratio $E(4_1^+)/E(2_1^+) = 2.6$ are fairly compatible with the expectations for a rotational band.

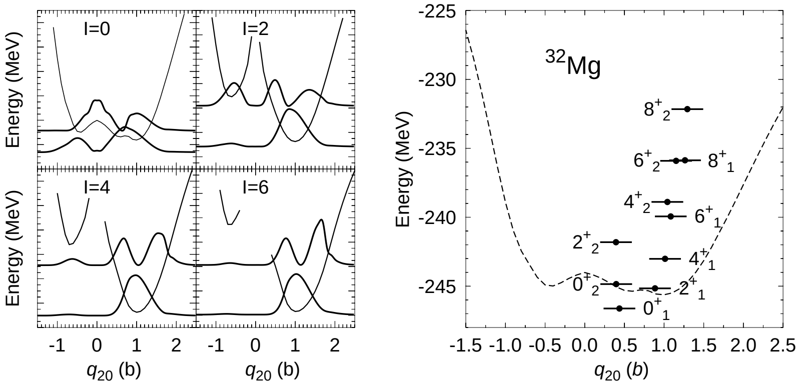

Fig. 7. On the left hand side, the square of the "collective wave functions" (in fact, $E^{I,\sigma} + 25|g^{I,\sigma}(q_{20})|^2$) for $\sigma = 1$ and 2 (thick lines) are plotted along with the corresponding projected energy (thin line) as a function of q_{20}. On the right hand side, the projected energies $E^{I,\sigma}$ along with the $I = 0$ projected energy are plotted as a function of q_{20}. The projected energies have been placed according to their average intrinsic quadrupole deformation $(\overline{q}_{20})^I_\sigma$

We have carried out Angular Momentum Projected configuration mixing calculations along the lines described in Sects. 2, 3 and 4. The AMP results have been already discussed in subsect. 3.5 and the AMPGCM ones are summarized in Fig. 7. On the left hand side of the figure we have plotted, as a function of q_{20} and for $I = 0$, 2, 4 and 6, and for practical reasons a quantity related to the square of the "collective wave functions", namely $E^I_\sigma + 25|g^{I,\sigma}(q_{20})|^2$, for $\sigma = 1$ and 2 as well as the projected energy curve. By looking at the tails of these quantities we can compare the AMPGCM energies E^I_σ with the corresponding projected energy and have a feeling of the correlation energy gained by configuration mixing. For $I = 0$ we observe how the ground state has an important mixing between the prolate and oblate minima. For $I = 2$, 4 and 6 the lowest lying solutions ($\sigma = 1$) are well localized inside the prolate wells whereas the excited solutions ($\sigma = 2$) show collective wave functions reminiscent of a β vibrational state. On the right hand side of Fig. 7 we have plotted the AMPGCM energies for $\sigma = 1$ and 2 along with the $I = 0$ projected energy. The AMPGCM energies have been placed along the q_{20} axis according to their "intrinsic average quadrupole moment" which is defined as the average quadrupole moment weighted with the "collective wave functions"

$$(\overline{q}_{20})^I_\sigma = \int dq_{20} q_{20} |g^{I,\sigma}(q_{20})|^2 \,. \tag{36}$$

As a result of the mixing with the oblate configurations, the 0^+_1 state has a lower intrinsic quadrupole deformation than the minimum of the $I = 0$ projected energy but remains strongly deformed indicating that the N=20 shell closure is broken in this nucleus. The intrinsic quadrupole deformation of the 2^+_1, 4^+_1 and 6^+_1 states remains similar the the one of the corresponding minima of the AMP energy curves as a consequence of the localization inside the prolate wells of their their collective wave functions. The 4^+_2, 6^+_2, etc, states have intrinsic quadrupole deformations similar to the 4^+_1, 6^+_1 ones in good agreement with its quadrupole vibrational character. Another interesting result is the low excitation energy of the 0^+_2 state which is related to the strong prolate-oblate mixing.

The results we have obtained with the AMPGCM for the 2^+ excitation energy and $B(E2, 0^+_1 \rightarrow 2^+_1)$ transition probability are 1.46 MeV and 395 e^2 fm^4, respectively. These results have to be compared with the angular momentum projected results obtained with the approximate PBV calculation discussed in Sect. 3.5 (0.87 MeV and 593 e^2 fm^4) and the experiment, 0.88 MeV and 454± 78 e^2 fm^4. As a consequence of configuration mixing the 2^+ excitation energy increases substantially as compared with the AMP result and differs considerably from the experimental number. However, the AMPGCM $B(E2)$ transition probability gets reduced with respect to the AMP result and gets closer to the experimental value.

^{32}Mg though an spherical nucleus in the mean field approximation represents the class of nucleus with a second minimum or a shoulder at an excitation energy comparable with the energy gain by AMP. A different case is provided by the nucleus ^{208}Pb already discussed or ^{48}Ca, see left panel of Fig. 8, which is also spherical at the mean field level but without any shoulder at relevant. The effect of the AMP in this case is to produce two almost degenerated prolate and oblate minima at small q values. The behavior of $\langle J_y^2 \rangle$ determine in part the energy gain of the ground state in the AMP, see Fig. 5 and the corresponding discussion, which is of the order of 3 MeV for ^{208}Pb and of 1 MeV for ^{48}Ca. In this case a configuration mixing calculation is called for which produces a ground state wave function which is a linear combination with similar weights of both minima and on the average

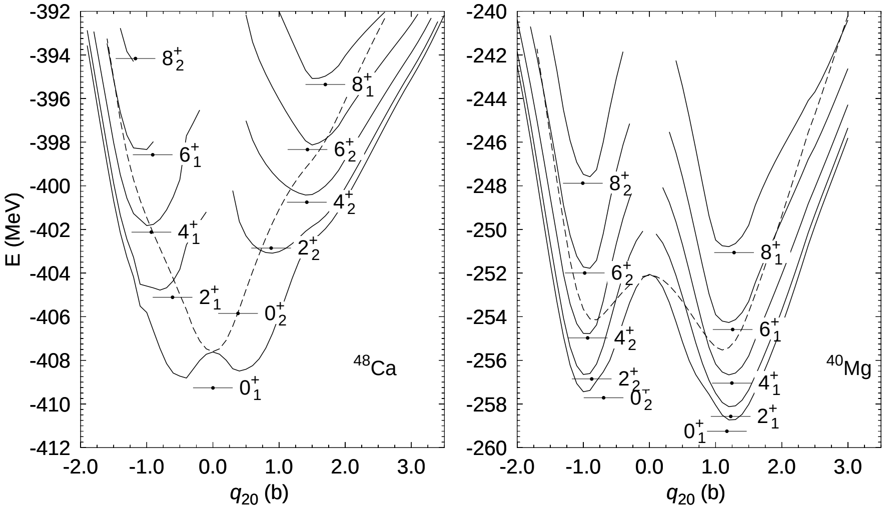

Fig. 8. The PES results for ^{48}Ca and ^{40}Mg for $I = 0, 2, 4, 6$ and 8, along with the HFB energy (dashed curves) as well as the AMPGCM results (see comments on the right panel of Fig. 7 for an explanation)

the ground state becomes again spherical, see Fig. 8. An additional energy gain (around 0.5 MeV in the case of ^{48}Ca) is also provided. For angular momentum 2, 4, 6 and 8 we find in Fig. 8 that the prolate and oblate minima of the PES of ^{48}Ca take place at larger deformations with increasing spins. This produces larger barriers between the minima and as a consequence the mixing get smaller with growing spins and the wave functions remain well localized in the corresponding minima. To complete our discussion we have plotted the mean field results, the PES and the AMPGCM energy levels in the right panel for the *well deformed* nucleus ^{40}Mg, though the REC's are similar for both plotted nuclei, the effect of the projection on the mean field energy is quite different. The MF prolate ground state and the secondary oblate minima, after the AMP remain approximately at the same q_{20} values and the same relative energy. The energy gain of the minima amounts to 3.5 MeV. The structure of the MFA energy surface is also roughly maintained by the PES at higher spins. The configuration mixing calculations provide different results than in the spherical nucleus, one obtain two rather well defined rotational bands, i.e., with rather constant intrinsic quadrupole moment, and less mixing in the wave functions. The energy gain of the ground state by the configuration mixing amounts about 600 keV.

In the following we will present results obtained with the Skyrme and the Gogny interaction. The calculations with the Skyrme interaction have been carried out mostly with the SLy4 [20] or the SLy6 [21] parameterizations of the force. In the AMPGCM ansatz a projection onto good particle number is also performed. In the case of the Gogny interaction the parameterization D1S [22] has been used. A simultaneous particle number projection has not been carried out because the finite range of the force considerably increases the computational burden as compared to the Skyrme interaction. As the field is pretty new there are not too many results and in some cases the nuclei computed with the Skyrme interaction are the same as the ones computed with the Gogny force. In those situations we will concentrate mainly in the Gogny results as the Skyrme ones are mostly in qualitative (and in some cases, quantitative) agreement with the former interaction. Most of the calculations have been focusing in light nuclei either with or without an excess of neutrons. Also calculations in heavier nuclei are available in the neutron deficient Lead isotopes although some more results will come in the near future.

We will start first commenting on the Skyrme results: the well deformed ^{24}Mg nucleus was discussed in [48] with the SLy4 force and zero range pairing interactions (depending and not depending on the density) and a reasonable agreement was obtained for the ground state rotational band although the band was too stretched. The intra-band $B(E2)$ transition probabilities were well reproduced. In [49] the doubly magic ^{16}O was studied with the SLy4 parameterization and focusing on the deformed 0^+ excited states and the corresponding rotational bands built on top of them. A rather good agreement was found between the calculations and the experimental results. The structure of the first excited 0^+ state was discussed in terms of multi particle-hole components and it was found that the structure of this state was a 4p-4h excitation in agreement with previous shell model explanations. It is interesting to point out that the ground state energy was lowered by 2.3 MeV with respect to the mean field as a consequence of the correlations induced by the AMPGCM method. The neutron deficient ^{186}Pb, which is a very nice example of shape coexistence with and spherical ground state and two excited states below 1 MeV of prolate and oblate character respectively, was studied in [50] with the SLy6 parameterization and zero range density dependent pairing interaction. The excitation energy of the prolate 0^+excited state was very well reproduced but this was not the case for the energy of the nearby oblate 0^+state. The rotational band built on top of the prolate 0^+ excited state came up too spread out as compared with the experimental data. The energies of both 0^+ states are pushed up to higher energies (1.05 MeV and 1.39 MeV for the prolate and oblate states, respectively) when the SLy4 force is used worsening the agreement with experiment. Finally, in [51] the nuclei ^{32}S, ^{36}Ar, ^{38}Ar and ^{40}Ca were studied. The interest was here the normal and super-deformed bands recently found in those nuclei. The normal deformed and super-deformed band heads come up at a reasonable excitation energy in all the nuclei but the rotational bands built on top of them come always too spread out as compared with the experiment. However, the $B(E2)$ values are in rather good agreement with experiment. The existence of SD bands in those nuclei is connected to a partial occupation of the $f_{7/2}$ sub-shell.

The calculations with the Gogny force have focused in neutron rich light nuclei in order to investigate the erosion of the $N = 20$ and $N = 28$ shell closures. To study the $N = 20$ region we computed [52] the Angular Momentum Projected energy curves for $^{30-34}$Mg and $^{32-38}$Si and from the minima of the projected curves we determined the lowest state for each angular momentum. In this way we were able to demonstrate that the ground state of the magic ^{32}Mg was deformed and traced back the breaking of the shell closure to the partial occupancy of the $f_{7/2}$ intruder orbital. We also obtained a deformed ground state in ^{34}Mg and for the other nuclei we concluded that they were showing shape coexistence. Concerning the excitation energy of the 2^+states we got a rather nice agreement with experiment as well as for the $B(E2)$ transition probabilities. From our preliminary analysis it was clear that a proper description of those nuclei should involve configuration mixing in the context of the AMPGCM. This calculation was carried out for $^{30-24}$Mg [53] and for $^{32-36}$Si [54]. As a general rule, the inclusion of configuration mixing increases the energy of the 2^+states as compared with the AMP results worsening the agreement with experiment but the $B(E2)$ get usually reduced improving the agreement with experiment. It was established the spherical character of ^{30}Mg and the deformed one of $^{32-34}$Mg as well as the spherical character of the ground states of all the Si isotopes studied.

To analyze the erosion of the $N = 28$ shell closure we have considered [55] the isotones from ^{40}Mg up to ^{48}Ca as well as the Sulfur isotopes $^{38-42}$S. It is found that the drip line nucleus ^{40}Mg is prolate deformed breaking thereby the $N = 28$ shell closure, the nucleus ^{42}Si is also deformed but in this case in the oblate side. The nuclei ^{44}S and ^{46}Ar are found to show shape coexistence whereas ^{48}Ca is found to be spherical as expected. Concerning the Sulfur isotopes they are found to be to a greater or lesser extent prolate deformed. The excitation energies of the 2^+states and specially their transition probabilities to the ground state are rather well reproduced (the energies always come up rather high as compared with the experiment). The two neutron and two protons separation energies are also well reproduced and it is found that the effect of AMPGCM is only significant in a few cases while in the other the results are pretty close to the HFB ones.

The Magnesium isotopic chain from A=20 until the neutron drip line A=40 was studied in [36]. The results obtained for the 2^+, $4^+$and 0_2^+ excitation energies as well as the $B(E2, 0^+ \to 2^+)$ are represented in Fig. 9 for the whole chain and compared with the experimental data. We observe that the isotopic trend is quite well reproduced but the $2^+$and 4^+ excitation energies come up too high whereas the 0_2^+ come up too low. Interestingly we are able to reproduce the sliding down of the 0_2^+excitation energy in going from ^{24}Mg to ^{26}Mg and due to the fact that whereas ^{24}Mg is a well deformed nucleus ^{26}Mg is a shape coexistent one [56]. One of the main results of our calculation is that the nuclei from ^{32}Mg to ^{40}Mg show a prolate deformed ground state. To finish the discussion of the Figure let us finally comment that the

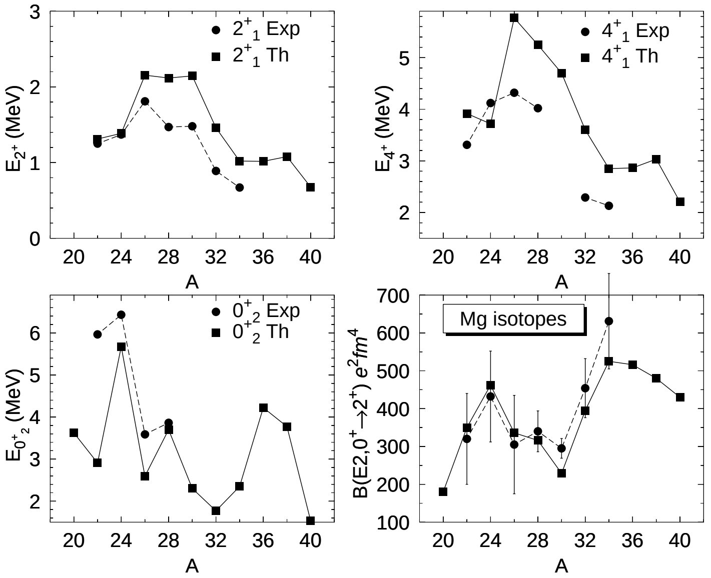

Fig. 9. Comparison of the theoretical results (full line) for the 2^+, 4^+, and 0_2^+ excitation energies and $B(E2, 0^+ \rightarrow 2^+)$ transition probabilities for the Mg isotopic chain with the experimental data (dashed line)

experimental $B(E2)$ transition probabilities are pretty well reproduced by our calculations.

The AMPGCM method not only provides the excitation energy of the states but also the ground state energy and therefore one can compute two neutron or two proton separation energies and compare them with the HFB results. This comparison is made in Fig. 10 for the Mg [36] and Ne [57] isotopic chains and there we observe how the AMPGCM method improves the agreement with experiment as compared with the HFB results. It is particularly interesting the $N = 22$ result that is strongly related to the erosion of the $N = 20$ shell closure, the inclusion of correlations that made ^{32}Mg deformed are the responsible for the better agreement of the S_{2N} separation energy in this case. Finally, let us mention that according to our calculations the neutron drip line for the Mg isotopes is located at $N = 28$. For the Ne isotopes the AMPGCM predicts (contrary to the mean field) an stable ^{32}Ne in good agreement with experiment.

Calculations similar to the ones presented for the Mg isotopes have also been carried out for the Ne isotopic chain in [57]. The conclusions are similar to the ones found for the Mg chain and they will not be discussed here.

Finally, let us comment on the fact that independently of the force used the rotational bands obtained with the AMPGCM method are too stretched as compared with the experimental data. On the other hand the $B(E2)$ tran-

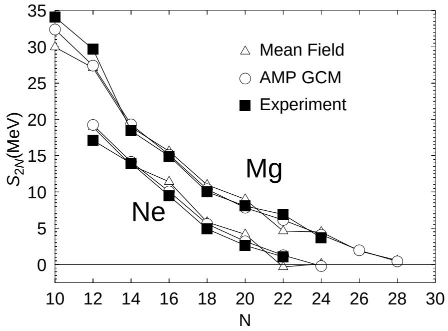

Fig. 10. Two neutron separation energies S_{2N} as a function of neutron number for the isotopic Mg and Ne chains. Results for the mean field and the AMPGCM calculations are present along with the experimental data

sition probabilities compare pretty well with experiment. This "feature" of the method might have to do with the lack in the present formalism of additional correlations like triaxialities, two-quasiparticle mixing and so on.

6 Outlook and Future Developments

In this paper we have described how to carry out Angular Momentum Projection (AMP) with effective interactions of the Skyrme and Gogny type. We have illustrated the procedure with several examples. The main outcome of those calculations is that AMP strongly modifies the energy landscape as a function of the mass quadrupole moment of the system and therefore the naive procedure of Projection After Variation (PAV) (i.e. projecting after the intrinsic state is determined at the mean field level by optimizing the intrinsic energy) leads in many cases to the wrong answer. On the other hand, the restricted Projection Before Variation (PBV) (i.e. the intrinsic state is determined by optimizing the projected energy) where only the quadrupole moment is allowed to vary yields much more consistent results. We have also learned that the projected energy landscapes have in many cases coexisting minima and therefore it is important to consider configuration mixing which is implemented in the framework of the Angular Momentum Projected Generator Coordinate Method (AMPGCM). The results shown indicate the relevance of configuration mixing in many cases. We have also discussed approximate ways to compute the projected quantities and in this context we have compared the present methodology with the results of the cranking model. All the methods considered have been illustrated with relevant examples and at the end we have given a rather exhaustive account of the available theoretical results. As the field is rather new there are still further improvements to be made: a) It has to be explored if there are other relevant degrees of freedom apart from the quadrupole moment that could be used in the context of the restricted PBV. b) The suitability of the method for the description of odd nuclei has to be explored. c) The octupole degree of freedom has to be incorporated in order to extend the present method into the realm of negative parity states. d) Triaxial and/or time reversal breaking admixtures have to be incorporated. e) Approximations to compute the projected quantities have to be explored and their suitability assessed, and a long etcetera !

7 Acknowledgements

All the work presented here for the Angular Momentum Projection plus Generator Coordinate Method with the Gogny force is part or an outcome of the Ph. D. thesis work of Rayner Rodríguez-Guzman to whom we are very indebted. This work has been supported in part by DGI, Ministerio de Ciencia y Tecnología, Spain, under Project BFM2001-0184.

References

1. M. Bender and P.-H. Heenen, Rev. of Mod. Phys. 75, 121 (2003)
2. H.J. Mang, Phys. Rep. 18, 325 (1975)
3. P. Ring and P. Schuck, *The Nuclear Many Body Problem* (Springer, Berlin, 1980)
4. J.-P. Blaizot and G. Ripka, *Quantum theory of Finite systems* (MIT, Cambridge, MA, 1985)
5. R.E. Peierls and J. Yoccoz, Proc. Phys. Soc. London **A**70, 381 (1957)
6. D.L.Hill and J.A.Wheeler, Phys. Rev. 89, 1102 (1953)
7. B.A. Brown, Prog. Part. Nucl. Phys. 47, 517 (2001)
8. E. Caurier, F. Nowacki, A. Poves and J. Retamosa, Phys. Rev. **C**58, 2033 (1998); A. Schmidt, I. Schneider, C. Friessner, A.F. Lisetskiy, N. Pietralla, T. Sebe, T. Otsuka and P. von Brentano, Phys. Rev. **C**62, 044319 (2000)
9. K.W. Schmid, Prog. Part. Nucl. Phys. 46, 145 (2001)
10. K.W. Schmid and F. Grümmer, Rep. Prog. Phys. 50, 731 (1987)
11. K. Hara and Y. Sun, Int. J. Mod. Phys. **E**4, 637 (1995)
12. T. Otsuka, M. Homma, T. Mizusaki, N. Shimizuo and Y. Utsuno, Prog. Part. Nucl. Phys. 47, 319 (2001)
13. T.H.R. Skyrme, Phil. Mag. 1, 1043 (1956); Nucl. Phys. 9, 615 (1959)
14. D. Vautherin and D.M. Brink, Phys. Rev. **C**3, 626 (1972)
15. Y.M. Engel, D.M. Brink K. Goeke, S.J. Krieger and D. Vautherin, Nucl. Phys. **A**249, 215 (1975)
16. J. Decharge and D. Gogny, Phys. Rev. **C**21, 1568 (1980)
17. M. Beiner, H. Flocard, Nguyen Van Giai and P. Quentin, Nucl. Phys. **A**238, 29 (1975)
18. H. Krivine, J. Treiner and O. Bohigas, Nucl. Phys. **A**366, 155 (1980)

19. J. Bartel, P. Quentin, M. Brack, C. Guet and H.-B Hakansson, Nucl. Phys. **A**386, 79 (1982)
20. E. Chabanat, P. Bonche, P. Haensel, J. Meyer and R. Schaeffer, Nucl. Phys. **A**627, 710 (1977)
21. E. Chabanat, P. Bonche, P. Haensel, J. Meyer and R. Schaeffer, Nucl. Phys. **A**635 (1998) 231; Nucl. Phys. **A**643, 441 (1998)
22. J.F. Berger, M. Girod and D. Gogny, Nucl. Phys. **A**428, 23c (1984)
23. M. Farine, D. Von-Eiff, P. Schuck, J. F. Berger, J. Dechargé and M. Girod, J. Phys. **G**: Nucl. Part. Phys. 25, 863 (1999)
24. M. Anguiano, J.L. Egido and L.M. Robledo, Nucl. Phys. **A**683, 227 (2001)
25. L. M. Robledo, Phys. Rev. **C**50, 2874 (1994); J.L. Egido, L.M. Robledo and Y. Sun, Nucl. Phys. **A**560, 253 (1993)
26. D. A. Varshalovich, A. N. Moskalev and V. K Khersonskii, *Quantum Theory of Angular Momentum* (World Scientific, Singapore, 1988)
27. J.O. Corbett, Nucl. Phys. **A**169, 426 (1971)
28. A.K. Kerman and N. Onishi, Nucl. Phys. **A**281, 373 (1977)
29. R.Balian and E.Brézin, *Il Nuovo Cimento*, vol. LXIV **B**, 37 (1969)
30. K.Neergard and E.Wust, Nucl. Phys. **A**402, 311 (1983)
31. P. Bonche, J. Dobaczewski, H. Flocard, P.-H. Heenen, Nucl. Phys. **A**530, 149 (1991)
32. K. Hagino, G.B. Bertsch and P.-G. Reinhard, Phys. Rev. **C**68, 024306 (2003)
33. T. Duguet and P. Bonche, Phys. Rev. **C**67, 054308 (2003)
34. P. Bonche, J. Dobaczewski, H. Flocard, P.-H. Heenen and J. Meyer, Nucl. Phys. **A**510, 466 (1990)
35. A. Valor, J.L. Egido and L.M. Robledo, Nucl. Phys. **A**665, 46 (2000)
36. R. Rodríguez-Guzmán, J.L. Egido and L.M. Robledo, Nucl. Phys. **A**709, 201 (2002)
37. F. Tondeur, S. Goriely, J.M. Pearson and M. Onsi, Phys. Rev. **C**62, 024308 (2000)
38. A. Kamlah, Z. Physik 216, 52 (1968)
39. R. Beck, H.J. Mang and P. Ring, Z. Physik 231, 26 (1970)
40. P.-G. Reinhard, Z. Physik **A**285, 93 (1978)
41. P.-G. Reinhard and K. Goeke, Rep. Prog. Phys. 50, 1 (1987)
42. W.A. Friedman and L. Wilets, Phys. Rev. **C**2, 892 (1970)
43. F. Villars and N. Schmeing-Rogerson, Annals of Physics 63, 433 (1971)
44. C. Détraz, D. Guillemaud, G. Huber, R. Plapisch, M. Langevin, F. Naulin, C. Thibault, L.C. Catraz and F. Touchard, Phys. Rev. **C**19 (1979) 164; D.Guillemaud-Mueller, C.Détraz, M.Langevin, F.Naulin, M.De Saint-Simon, C.Thibault, F.Touchard and M.Epherre, Nucl. Phys. **A**426, 37 (1984)
45. G. Klotz, P. Baumann, M. Bounajma, A. Huck, A. Knipper, G. Walter, G. Marguier, C. Richard-Serre, A. Poves and J. Retamosa, Pys. Rev. **C**47, 2502 (1993)
46. D. Guillemaud-Mueller, Eur. Phys. J. **A** 13, 63 (2002)
47. T.Motobayashi, Y.Ikeda, Y.Ando, K.Ieki, M.Inoue, N.Iwasa, T.Kikuchi, M.Kurokawa, S.Moriya, S.Ogawa, H.Murakami, S.Shimoura, Y.Yanagisawa, T.Nakamura, Y.Watanabe, M.Ishiara, T.Teranishi, H.Okuno and R.F.Casten, Phys. Lett. **B**346, 9 (1995)
48. A. Valor, P.-H. Heenen and P. Bonche, Nucl. Phys. **A**671, 145 (2000)
49. M. Bender and P.-H. Heenen, Nucl.Phys. **A**713, 390 (2003)

50. T. Duguet, M. Bender, P. Bonche and P.-H. Heenen, Phys.Lett. **B**559, 201 (2003)
51. M. Bender, H. Flocard and P.-H. Heenen, (*preprint nucl-th/0305021*)
52. R. Rodríguez-Guzmán, J.L. Egido and L.M. Robledo, Phys. Lett. **B**474, 15 (2000)
53. R. Rodríguez-Guzmán, J.L. Egido and L.M. Robledo, Phys. Rev. **C**62, 054319 (2000)
54. R. Rodríguez-Guzmán, J.L. Egido and L.M. Robledo, Acta Phys. Pol. **B**32, 2385 (2001)
55. R. Rodríguez-Guzmán, J.L. Egido and L.M. Robledo, Phys. Rev. **C**65, 024304 (2002)
56. R. Rodríguez-Guzmán, J.L. Egido and L.M. Robledo, AIP *Conference Proceedings* 656, 303 (2003)
57. R. Rodríguez-Guzmán, J.L. Egido and L.M. Robledo, Eur. Phys. J. **A**17, 37 (2003)